An unexpected reactivity of the P$_{460}$ cofactor in hydroxylamine oxidoreductase

Andreas Dietl,[a] Wouter Maalcke[b] and Thomas R. M. Barends[a]*

[a]Department of Biomolecular Mechanisms, Max Planck Institute for Medical Research, Jahnstrasse 29, 69120 Heidelberg, Germany, and [b]Department of Microbiology, Institute for Water and Wetland Research, Radboud University, 6525 AJ Nijmegen, The Netherlands. *Correspondence e-mail: thomas.barends@mpimf-heidelberg.mpg.de

Hydroxylamine oxidoreductases (HAOs) contain a unique haem cofactor called P$_{460}$ that consists of a profoundly ruffled c-type haem with two covalent bonds between the haem porphyrin and a conserved tyrosine. This cofactor is exceptional in that it abstracts electrons from a ligand bound to the haem iron, whereas other haems involved in redox chemistry usually inject electrons into their ligands. The effects of the tyrosine cross-links and of the haem ruffling on the chemistry of this cofactor have been investigated theoretically but are not yet clear. A new crystal structure of an HAO from *Candidatus* Kuenenia stuttgartiensis, a model organism for anaerobic ammonium oxidation, now shows that its P$_{460}$ cofactor has yet another unexpected reactivity: when ethylene glycol was used as a cryoprotectant, the 1.8 Å resolution electron-density maps showed additional density which could be interpreted as an ethylene glycol molecule covalently bound to the C$_{16}$ atom of the haem ring, opposite the covalent links to the conserved tyrosine. Possible causes for this unexpected reactivity are discussed.

1. Introduction

Octahaem hydroxylamine oxidoreductases (HAOs) catalyse the oxidation of hydroxylamine (NH_2OH) to nitrite (NO_2^-) or nitric oxide (NO). The active sites of these proteins contain a unique, modified haem cofactor called P$_{460}$ owing to its characteristic peak around 460 nm in the UV–Vis spectra of the dithionite-reduced protein (Erickson & Hooper, 1972). P$_{460}$ consists of a c-type haem that is covalently linked to a conserved tyrosine residue (Arciero *et al.*, 1993). Among haem redox cofactors, P$_{460}$ is exceptional in that it abstracts protons from a ligand bound to the iron, whereas other haems involved in redox chemistry usually inject electrons into their iron-bound ligands. Thus, there has been considerable interest in investigating the detailed structure of this cofactor with a view to explaining this deviation from typical haem redox chemistry.

The first structural information on P$_{460}$ based on mass spectrometry and NMR spectroscopy reported by Arciero and coworkers was consistent with a single covalent bond between a haem *meso* C atom and a tyrosine-ring C atom in the *meta* position (Arciero *et al.*, 1993). Later, the 2.8 Å resolution crystal structure of the HAO from *Nitrosomonas europaea* indeed showed a covalent link between the porphyrin ring and the side chain of a conserved tyrosine. At the time, the structure of the P$_{460}$ cofactor determined at this medium resolution was modelled with a single covalent bond between the haem C$_5$ and the C$^\varepsilon$ atom, probably influenced by the results obtained by Arciero and coworkers (Igarashi *et al.*, 1997). Later, however, the 2.1 Å resolution crystal structure of
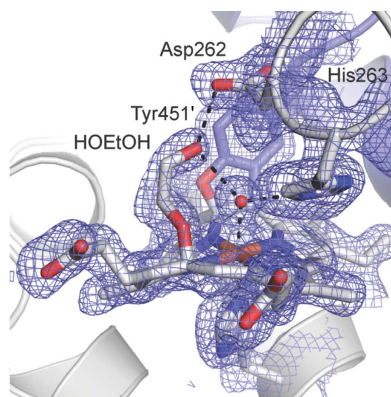

Asp262
His263
Tyr451'
HOEtOH

Table 1
Crystallization.

Method	Hanging-drop vapour diffusion
Plate type	24-well Linbro plate, glass cover slip
Temperature (K)	293
Protein concentration	$A_{280}^{1\,cm} = 20$ ($A_{409}^{1\,cm} = 95$)
Buffer composition of protein solution	25 mM HEPES–KOH pH 7.5, 25 mM KCl
Composition of reservoir solution	1.3 M ammonium sulfate, 0.05–0.1 M sodium phosphate buffer pH 7.4, 35 mM C-HEGA-10
Volume and ratio of drop	1 µl + 1 µl
Volume of reservoir (µl)	800

the *Nitrosomonas* HAO (Cedervall *et al.*, 2013), as well as the 1.8 Å resolution crystal structure of the HAO from *Candidatus* Kuenenia stuttgartiensis (Maalcke *et al.*, 2014) published shortly afterwards, both clearly showed a second covalent bond between the C_4 atom of the porphyrin macrocycle and the O^η atom of the tyrosine (Fig. 1). As shown in all available crystal structures of HAOs, the covalent attachment to the tyrosine results in a high degree of ruffling of the haem porphyrin macrocycle.

A theoretical study of the HAO mechanism (Fernández *et al.*, 2008) suggested that the unusual electron-abstracting reactivity of P_{460} is assisted by the presence of the tyrosine residue through the destabilization of a haem–nitric oxide intermediate in which the combined number of iron d and NO π^* electrons is seven; it is therefore denoted the {FeNO}^{7} complex (Enemark & Feltham, 1974). The destabilization of this intermediate favours its transformation into an {FeNO}^{6} intermediate by the removal of an electron. However, these calculations were based on the 2.8 Å resolution crystal structure and thus assumed only one covalent bond between the haem porphyrin and the tyrosine. Therefore, it is not yet exactly clear what causes P_{460} to deviate from typical haem redox chemistry.

Here, we report another unexpected reactivity of P_{460}. In order to obtain the native structure of the HAO from *Candidatus* K. stuttgartiensis (Maalcke *et al.*, 2014), crystals were cryoprotected using sucrose. We now present the structure of HAO determined using ethylene glycol as the cryoprotectant. In this structure, an ethylene glycol molecule is covalently bound to the P_{460} cofactor at the C_{16} atom of the haem moiety. This observation, while probably an artefact, illustrates the pronounced effects of the haem ruffling on the chemistry of the porphyrin ring of P_{460}.

2. Materials and methods

2.1. Protein crystallization

Candidatus K. stuttgartiensis HAO was purified as described earlier and crystallized as reported in Maalcke *et al.* (2014). Briefly, crystals were grown at room temperature in hanging-drop vapour-diffusion setups using 1.3 M ammonium sulfate in 0.05–0.1 M sodium phosphate buffer with 35 mM cyclohexylbutanoyl-*N*-hydroxyethylglucamide (C-HEGA-10) as the reservoir solution. Dark red rhombic dodecahedra grew

Table 2
Data collection and processing.

Values in parentheses are for the outer shell.

Diffraction source	PXII, SLS
Wavelength (Å)	1.0000
Temperature (K)	100
Detector	Pilatus 6M
Crystal-to-detector distance (mm)	260
Rotation range per image (°)	0.25
Total rotation range (°)	60
Exposure time per image (s)	0.25
Space group	$P2_13$
a, b, c (Å)	130.3, 130.3, 130.3
α, β, γ (°)	90, 90, 90
Mosaicity (°)	0.131
Resolution range (Å)	20–1.8 (1.9–1.8)
Total No. of reflections	459071 (68470)
No. of unique reflections	68117 (10121)
Completeness (%)	99.7 (99.9)
Multiplicity	6.7 (6.8)
$\langle I/\sigma(I) \rangle$	19.6 (3.9)
$R_{r.i.m.}$ (%)	7.3 (52.0)
Overall B factor from Wilson plot (Å^2)	26.9

to a diameter of 150 µm within 3 d. Crystallization information is summarized in Table 1. One of these crystals was flash-cooled in liquid nitrogen after soaking for 5 min in an artificial reservoir solution containing 25%(v/v) ethylene glycol and stored in liquid nitrogen for subsequent data collection. Data-collection and processing statistics are summarized in Table 2.

2.2. Data collection and structure solution

A 1.8 Å resolution data set was collected on the PXII beamline of the Swiss Light Source at the Paul Scherrer Institute, Villigen, Switzerland. The data were processed in *XDS* (Kabsch, 2010*a,b*) and phased by molecular replacement using *Phaser* (McCoy *et al.*, 2007; McCoy, 2007) with the known *Candidatus* K. stuttgartiensis HAO crystal structure (Maalcke *et al.*, 2014) and the structure was refined using *REFMAC*5 (Murshudov *et al.*, 1997, 2011). Geometrical parameters for the P_{460} cofactor and for its covalent bond to an ethylene glycol molecule were obtained from semi-empirical quantum-chemical calculations at the PM-3 level (Steward, 1989) using *HyperChem* 8.0. Coordinates and structure-factor amplitudes have been deposited in the
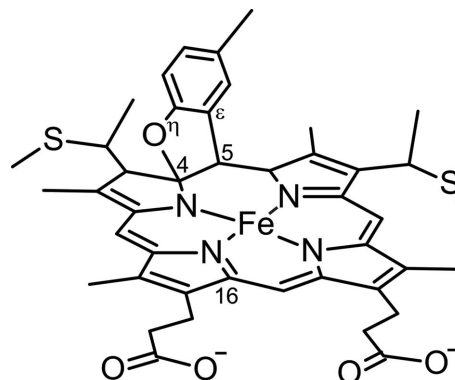

Figure 1
Structure of the P_{460} cofactor. The porphyrin C atoms C_4, C_5 and C_{16} are indicated, as well as the tyrosine O^η and C^ε.

Table 3
Structure solution and refinement.

Values in parentheses are for the outer shell.

Resolution range (Å)	46.1–1.8 (1.9–1.8)
Completeness (%)	99.7 (99.9)
σ Cutoff	None
No. of reflections, working set	64753 (4748)
No. of reflections, test set	3364 (288)
Final R_{cryst}	0.147 (0.197)
Final R_{free}	0.164 (0.250)
Cruickshank DPI	0.0880
No. of non-H atoms	
Protein	3945
Ion	15 [3 PO_4^{3-}]
Ligand	344 [8 haem], 12 [1 C-HEGA-10], 20 [5 ethylene glycol]
Water	509
Total	4845
R.m.s. deviations	
Bonds (Å)	0.007
Angles (°)	1.091
Average B factors (Å^2)	
Overall	15.3
Protein	18.8
Ion/ligand	16.4
Water	28.2
Ramachandran plot	
Most favoured (%)	96.2
Allowed (%)	3.6
Disallowed (%)	0.2†

† This is the conserved His263 which is in a strained conformation.

Protein Data Bank as entry 4rwm. Refinement statistics are summarized in Table 3.

2.3. UV–Vis spectroscopy

For the acquisition of qualitative spectra, the protein was diluted to $A_{280} \simeq 0.2$ and $A_{409} \simeq 0.9$ in 100 mM sodium phosphate buffer solution pH 7.4. Spectra of the reduced enzyme were recorded in 1 ml quartz cuvettes with a 1.0 cm path length (Hellma GmbH, Müllheim, Germany) at 0.5 nm bandwidth using a Jasco V-650 spectrophotometer (Jasco GmbH, Gross-Umstadt, Germany) equipped with a thermostatted sample holder at 25°C. The data were processed using the *Jasco*32 software. The protein was reduced by the addition of a few crystals of solid sodium dithionite ($Na_2S_2O_4$) to the samples (1 ml volume) and spectra were recorded in the presence and absence of 10%(v/v) ethylene glycol.

3. Results and discussion

No large-scale differences were observed between the crystal structures of native *Candidatus* K. stuttgartiensis HAO using either sucrose or ethylene glycol as the cryoprotectant. In both cases the asymmetric unit contained one monomer and the haem part of the P_{460} cofactor appeared to be highly ruffled to a similar extent owing to the two covalent bonds between the porphyrin macrocycle C_4 and C_5 atoms and the O^η and C^ε atoms, respectively, of the conserved tyrosine residue Tyr451′ from an adjacent monomer in the trimer (Maalcke *et al.*, 2014). However, in the electron-density maps of the ethylene glycol structure additional density was present close to the haem C_{16}

atom of the P_{460} cofactor (Figs. 2a and 2b), indicating that a small molecule had bound to the haem group. Moreover, the density showed that the side chain of Asp262 of the conserved Asp/His pair had rotated away to accommodate the new molecule bound to the haem (Figs. 2a, 2b and 2c). Given the size, shape and position of the density, and considering the various components of the mother liquor and cryoprotection solution for the crystal, the most likely explanation of the density appeared to be a single ethylene glycol molecule covalently bound to the haem C_{16} C atom with one of its O atoms (Fig. 2). The ethylene glycol was only included at a late stage in the refinement and was modelled with full atom occupancies. The B factors for the ethylene glycol refined to an average value of 24.5 Å^2, which is somewhat higher than the average B factor of the P_{460} cofactor (16.3 Å^2), suggesting that the occupancy was less than 1.0 in the crystal. The refined distance between C_{16} and the ethylene glycol O atom is 1.46 Å, which is in the range of covalent C—O bond lengths, and is close to the expected value of 1.43 Å obtained from semi-empirical calculations at the PM-3 level (Steward, 1989). The C_{16}-atom geometry can be described as a distorted tetrahedron with angles between the ethylene glycol O atom and the substituents around C_{16} of between 94 and 99°. The refined geometry of the P_{460}–ethylene glycol adduct is very similar to the semi-empirically optimized geometry (Fig. 2d).

Importantly, in the 1.8 Å resolution native data set reported in Maalcke *et al.* (2014), which was collected from a crystal cryoprotected using 30%(w/v) sucrose in the mother liquor, no additional density bound to C_{16} was observed, which is consistent with this density being caused by an ethylene glycol molecule. Moreover, UV–Vis spectra of reduced *Candidatus* K. stuttgartiensis HAO in the presence of 10%(v/v) ethylene glycol did not show the characteristic P_{460} absorption peak, which in *Candidatus* K. stuttgartiensis HAO is at 468 nm, whereas this absorption is clearly present in spectra of the reduced enzyme without ethylene glycol (Fig. 3).

Importantly, the complex structures of *Candidatus* K. stuttgartiensis HAO soaked in hydroxylamine, hydrazine and phenylhydrazine reported in Maalcke *et al.* (2014) were also obtained using ethylene glycol as the cryoprotectant in the ligand-soaking solution. However, in these cases no additional density was observed for an ethylene glycol molecule bound to the haem. It is probable that complex formation with hydroxylamine, hydrazine and phenylhydrazine occurs before ethylene glycol adduct formation and prohibits it, either by reducing the haem or by steric hindrance between the iron ligand and the ethylene glycol.

Apart from the difference density for the ethylene glycol moiety and the rotated side chain of Asp262, there is also difference density suggesting that the distal water molecule in the ethylene glycol-soaked structure is closer to the haem iron (Fe—O distance of 2.2 Å) than in the sucrose-soaked structure (Fe—O distance of 2.5 Å). This is probably owing to partial reduction of the sucrose-soaked crystal (Beitlich *et al.*, 2007) caused by radiation damage during data collection.

The mechanism of ethylene glycol addition to the P_{460} cofactor is unclear. In aqueous solution at approximately
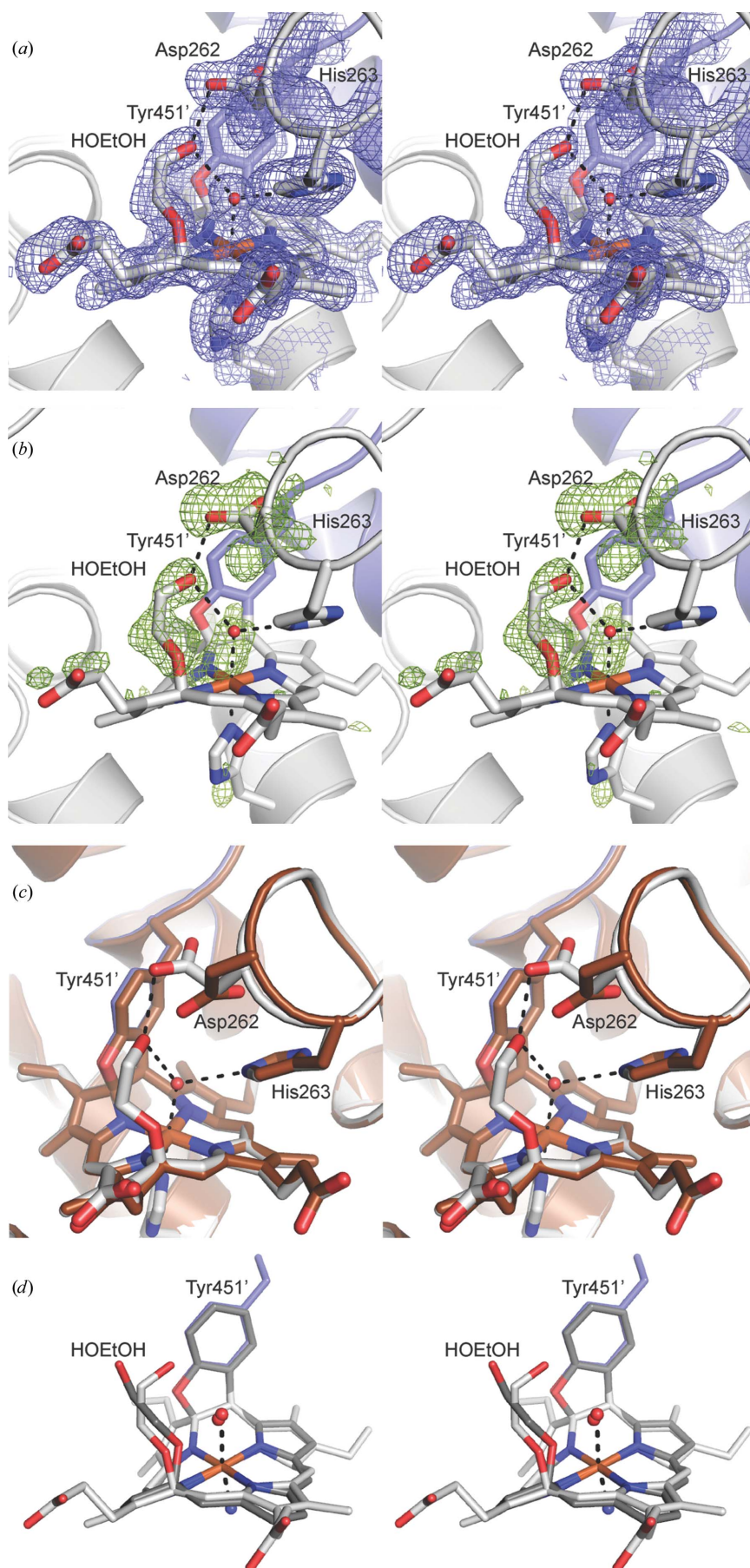
neutral pH, ethylene glycol is not a
particularly reactive molecule. Indeed,
for the addition of polyethylene glycol
to proteins ('PEGylation'), the PEG
hydroxyl groups need to be activated
using, for example, cyanuric chloride
or other highly reactive compounds
(Roberts *et al.*, 2012). Oxidation of
ethylene glycol results in the formation
of glycolaldehyde (2-hydroxyethanal),
which may be expected to be more
reactive, however, and the possibility
that glycolaldehyde causes the observed
reaction cannot be excluded. Further
oxidation would result in the formation
of carboxylic acids such as glycolic acid.
However, the reaction of such a
compound with the P_{460} cofactor would
most likely have resulted in an ester-
type bond, and despite the high resolu-
tion the electron density offers no
evidence for such an adduct.

Covalent adducts of haem groups are
well known; haem *c* cofactors are by
definition covalently bound to the
protein *via* thioether bonds between the
vinyl groups of the haem and cysteine
residues, and in haem *d* a propionate
group can form a *γ*-spirolactone with a
C atom of the porphyrin ring (Sotiriou
& Chang, 1988; Murshudov *et al.*, 1996).

Figure 2
Stereofigures showing (*a*) the simulated-
annealing composite OMIT ($2mF_o - DF_c$, blue,
1.5σ) and (*b*) the $mF_o - DF_c$ (green, +3σ)
electron-density maps (Read, 1986) for the P_{460}
cofactor in an ethylene glycol-soaked *Candi-
datus* K. stuttgartiensis HAO crystal. The maps
were calculated by *PHENIX* (Adams *et al.*,
2010) using the native structure (PDB entry
4n4j; Maalcke *et al.*, 2014) after rigid-body
refinement, in which ethylene glycol is not
included. The maps are superimposed on the
final, refined structure. The conserved Asp262/
His263 pair involved in proton abstraction
from the substrate (Maalcke *et al.*, 2014) is
indicated, and the double covalent link
between the P_{460} cofactor and Tyr451' from
another subunit (blue) can be seen in the
background. (*c*) Superposition of the native
structure (brown) onto the final, refined
structure of the ethylene glycol adduct struc-
ture (grey). The side chain of Asp262 has been
displaced by the presence of the ethylene glycol
molecule. (*d*) Superposition of the P_{460} cofactor
as observed in the crystal structure of the
ethylene glycol adduct (light grey) and the
PM-3 optimized cofactor (dark grey). An
ammonia molecule was used to model the
proximal histidine ligand in the semi-empirical
optimization (blue sphere) and the propionates
were omitted.

There are also several examples of covalent modifications at haem *meso* C atoms: Arciero & Hooper (1997) found a covalent link between a lysine residue and a *meso* C atom of a *c*-type haem in the *N. europaea* monohaem cytochrome P460. This was subsequently confirmed by the crystal structure of this protein determined by Pearson *et al.* (2007), who also found a hydroxyl adduct to a *meso* C atom when the protein was heavily oxidized. Haem oxygenase selectively oxidizes the α-*meso* atom as the first step in haem degradation (Schuller *et al.*, 1999; Matsui *et al.*, 2005). The incubation of horseradish peroxidase with H_2O_2 and chloride resulted in the addition of a chlorine to a haem *meso* atom (Huang *et al.*, 2005), and the reaction of myoglobin with alkyl hydrazines results in alkylation at the γ-*meso* atom (Choe & Ortiz de Montellano, 1991).

Thus, while there are several examples of haem modifications at either the vinyl groups or *meso* C atoms, there are few examples of modifications at the pyrrole C atoms flanking the N atoms such as C_{16}, suggesting these atoms to be comparatively nonreactive under most circumstances.

Apparently, in P_{460} the pronounced ruffling caused by the covalent bonds between haem and tyrosine has increased the reactivity of the C_{16} atom towards ethylene glycol. In a planar, undistorted porphyrin ring, the C_{16} atom would have mainly sp^2 character. In P_{460}, the ruffling is likely to cause the C_{16} atom, which is opposite the covalent bonds to the tyrosine, to adopt a more sp^3-like geometry, increasing its reactivity by straining the local structure. Moreover, the remaining hydroxyl group of the ethylene glycol moiety is bound to the side-chain carboxylate group of the conserved Asp262 *via* a hydrogen bond (Fig. 2). In this way, the protein could assist in adduct formation by binding ethylene glycol in a favourable position and orientation.

Whether the observed adduct has any biological relevance in itself appears doubtful; ethylene glycol is chemically very different from the putative substrate hydroxylamine. However, since this unexpected reactivity of the P_{460} cofactor is likely to be caused by the effects of the ruffling induced by the bonds to Tyr451′ on the chemistry of the porphyrin ring, this observation may assist in elucidating the electronic properties of the P_{460} cofactor, which in turn could shed light on the unique reversal of the electron-flow direction in this singular haem cofactor.
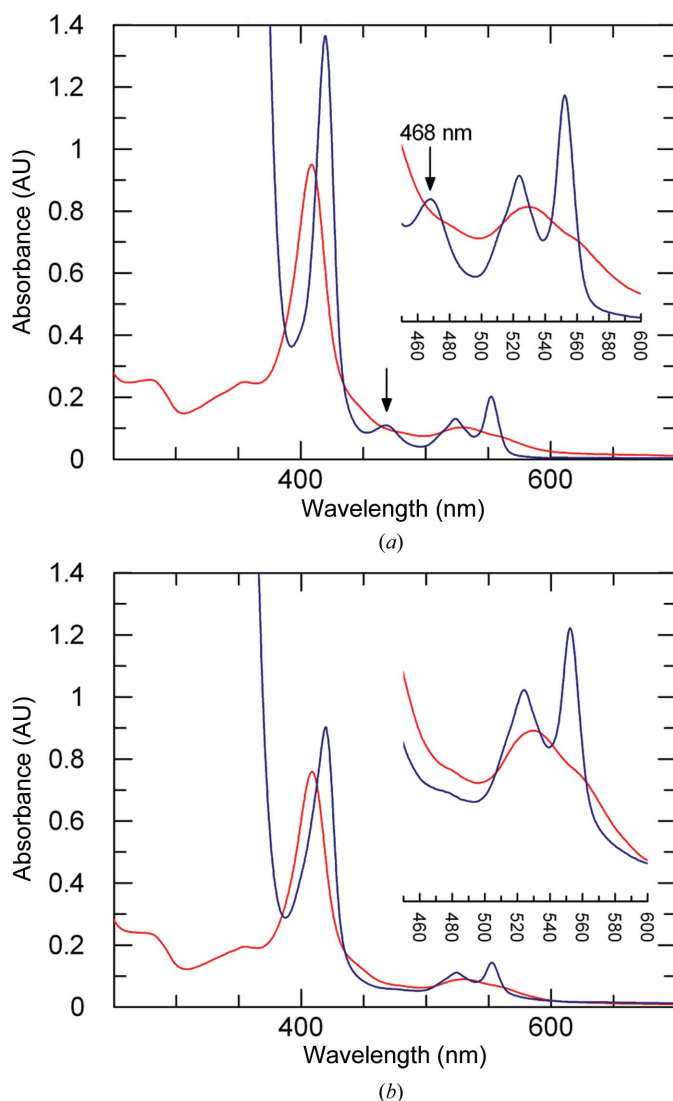
Figure 3
Spectra of the *Candidatus* K. stuttgartiensis HAO protein as isolated (red lines) and after reduction with dithionite (blue lines). The insets show the details of the spectra between 450 and 600 nm. Spectra were measured without ethylene glycol (*a*) and in the presence of 10%(*v*/*v*) ethylene glycol (*b*). The characteristic 468 nm absorption upon reduction (black arrows) is not observed when 10%(*v*/*v*) ethylene glycol is present.

References

Adams, P. D. *et al.* (2010). *Acta Cryst.* D**66**, 213–221.
Arciero, D. M. & Hooper, A. B. (1997). *FEBS Lett.* **410**, 457–460.
Arciero, D. M., Hooper, A. B., Cai, M. & Timkovich, R. (1993). *Biochemistry*, **32**, 9370–9378.
Beitlich, T., Kühnel, K., Schulze-Briese, C., Shoeman, R. L. & Schlichting, I. (2007). *J. Synchrotron Rad.* **14**, 11–23.
Cedervall, P., Hooper, A. B. & Wilmot, C. M. (2013). *Biochemistry*, **52**, 6211–6218.
Choe, Y. S. & Ortiz de Montellano, P. R. (1991). *J. Biol. Chem.* **266**, 8523–8530.
Enemark, J. H. & Feltham, R. D. (1974). *Coord. Chem. Rev.* **13**, 339–406.
Erickson, R. H. & Hooper, A. B. (1972). *Biochim. Biophys. Acta*, **275**, 231–244.
Fernández, M. L., Estrin, D. A. & Bari, S. E. (2008). *J. Inorg. Biochem.* **102**, 1523–1530.
Huang, L. S., Wojciechowski, G. & Ortiz de Montellano, P. R. (2005). *J. Am. Chem. Soc.* **127**, 5345–5353.
Igarashi, N., Moriyama, H., Fujiwara, T., Fukumori, Y. & Tanaka, N. (1997). *Nature Struct. Mol. Biol.* **4**, 276–284.
Kabsch, W. (2010*a*). *Acta Cryst.* D**66**, 133–144.

Kabsch, W. (2010*b*). *Acta Cryst.* D**66**, 125–132.

Maalcke, W. J., Dietl, A., Marritt, S. J., Butt, J. N., Jetten, M. S., Keltjens, J. T., Barends, T. R. M. & Kartal, B. (2014). *J. Biol. Chem.* **289**, 1228–1242.

Matsui, T., Furukawa, M., Unno, M., Tomita, T. & Ikeda-Saito, M. (2005). *J. Biol. Chem.* **280**, 2981–2989.

McCoy, A. J. (2007). *Acta Cryst.* D**63**, 32–41.

McCoy, A. J., Grosse-Kunstleve, R. W., Adams, P. D., Winn, M. D., Storoni, L. C. & Read, R. J. (2007). *J. Appl. Cryst.* **40**, 658–674.

Murshudov, G. N., Grebenko, A. I., Barynin, V., Dauter, Z., Wilson, K. S., Vainshtein, B. K., Melik-Adamyan, W., Bravo, J., Ferrán, J. M., Ferrer, J. C., Switala, J., Loewen, P. C. & Fita, I. (1996). *J. Biol. Chem.* **271**, 8863–8868.

Murshudov, G. N., Skubák, P., Lebedev, A. A., Pannu, N. S., Steiner, R. A., Nicholls, R. A., Winn, M. D., Long, F. & Vagin, A. A. (2011). *Acta Cryst.* D**67**, 355–367.

Murshudov, G. N., Vagin, A. A. & Dodson, E. J. (1997). *Acta Cryst.* D**53**, 240–255.

Pearson, A. R., Elmore, B. O., Yang, C., Ferrara, J. D., Hooper, A. B. & Wilmot, C. M. (2007). *Biochemistry*, **46**, 8340–8349.

Read, R. J. (1986). *Acta Cryst.* A**42**, 140–149.

Roberts, M. J., Bentley, M. D. & Harris, J. M. (2012). *Adv. Drug Deliv. Rev.* **64**, 116–127.

Schuller, D. J., Wilks, A., Ortiz de Montellano, P. R. & Poulos, T. L. (1999). *Nature Struct. Biol.* **6**, 860–867.

Sotiriou, C. & Chang, C. K. (1988). *J. Am. Chem. Soc.* **110**, 2264–2270.

Steward, J. J. P. (1989). *J. Comput. Chem.* **10**, 221–264.